# Mononuclear copper(I) complexes bearing 3-phenyl-5-(pyridin-4-yl)-1, 2, 4-triazole ligand: synthesis, crystal structure, TADF-luminescence, and mechanochromic effects

*Alexey Gusev, Elena Braga, Ekaterina Zamnius, Mikhail Kiskin, Amjad Ali, Glib Baryshnikov, Wolfgang Linert*

## List of Content

# 1. Computational Details

The density functional theory (DFT) and time-dependent (TD) DFT calculations were performed with Gaussian 16 software.[1] The chemical structures of complexes **1**, **2**, and **3** in the ground electronic state (S0) were optimized at the density functional theory (DFT) level in the acetonitrile (CH3CN) using the B3LYP functional and 6-311G(d, p) basis set [2-6] for C, H, P, N, and O atoms and LANL2DZ effective core potential (ECP) for Cu and halogens.[7, 8] The vibrational frequencies were confirmed for both ground and excited state optimizations and no imaginary frequencies were found. The first excited singlet (S1) and triplet (T1) state calculations have been carried out using the PBE0[9, 10] functional with 6-311G(d,p) and LANL2DZ ECP for two different groups of atoms in the same up-mentioned manner for the ground-state. The global hybrid PBE0 functional with 25% Hartree-Fock exact exchange is known for calculation of the excited-state properties of optoelectronic materials.[11-15] The structures of all complexes in the S1 and T1 state were optimized by the TD-DFT method using the Tamm-Dancoff approximation (TDA)[16] at the GD3-PBE0/6-311G(d,p) level. Additionally, we optimized T1 state geometries of the studied complexes with the spin-unrestricted GD3-UPBE0/6-311G(d,p) formalism. The excited-state calculations were all performed in acetonitrile (CH3CN) as a model solvent. The Polarizable Continuum Model (PCM)[17] was used to consider the solvent effect for S0, S1 and T1 states of all molecules. The Grimme's dispersion correction was accounted during S0, S1, and T1 states optimization at the GD3 level.[18] Based on the S1 and T1 state optimized coordinates of chemical structures, the spin-orbit coupling (SOC) effect was treated as a perturbation based on the scalar relativistic (SR) orbitals after SCF and TDDFT calculations (pSOC-TDDFT)[19] using the ADF software (version 2021.102).[20] The SOC matrix elements $\langle S1|\hat{H}SO|T1 \rangle$ were calculated as root mean squares at S1 state geometry, i.e. as square

root of the sum of squares of spin-orbit coupling matrix elements of all triplet state sublevels ($m=0,\pm1$) of the uncoupled states:

$$\langle S_1 | \hat{H}_{SO} | T_1 \rangle = \sqrt{\sum_{m = 0, \pm 1} \langle S_1 | \hat{H}_{SO} | T_1^m \rangle^2}$$

(1)

The spin-orbit coupling operator $\hat{H}_{SO}$ was considered in our calculations within the zeroth-order regular approximation (ZORA).[21] The fluorescence rate constants ($k_{flu}$) for all complexes were predicted according to the following relationship:

$$k_{flu} = \frac{1}{\tau_{av}} = \frac{2(\Delta E^2)f}{c^3}$$

(2)

where $\Delta E$ and $f$ – the energy and intensity of the corresponding singlet-singlet transition – were calculated at the S1 state geometry with account of SOC perturbations.

The average phosphorescence lifetime ($\tau_{av}$) for $T_1^m$ sublevels of all the three complexes was estimated using the following averaging formula:

$$\tau_{av(phos)} = \frac{3}{(\frac{1}{\tau_x} + \frac{1}{\tau_y} + \frac{1}{\tau_z})}$$

(3)

Based on $\tau_{av}$ value the averaged phosphorescence rate constant ($k_{phos}$) was estimated following the inverse $\tau_{av} = 1/k_{phos}$ relation.

The rates of intersystem crossing (ISC) and reverse intersystem crossing (RISC) were estimated using semiclassical Marcus theory expression:[22]

$$k_{(R)ISC} = \frac{2\pi}{\hbar} \langle S_1 | \hat{H}_{SO} | T_1 \rangle^2 \sqrt{\frac{1}{4\pi k_b T \lambda}} exp[-\frac{(\Delta E_{ST} + \lambda)^2}{4k_b T \lambda}]$$

(5)

where $k_b$ is the Boltzmann constant, T is the temperature, which is set to 298 K, $\Delta E_{ST}$ is adiabatic excitation energy difference, $\lambda$ is the reorganization energy induced by S1-T1 ISC or T1-S1 RICS. $\Delta E_{ST} < 0$ for the $k_{ISC}$ rate, while for RISC $\Delta E_{ST}$ is negative with the same magnitude (i.e. $\Delta E_{ST} > 0$). Similarly, the different reorganization energies were used for $k_{ISC}$ and $k_{RISC}$ named as $\lambda_T$ and $\lambda_S$, respectively:

$$\lambda_T = E(T_1)^{S_1\,geom} - E(T_1)^{T_1\,geom} \qquad (7)$$

$$\lambda_S = E(S_1)^{T_1\,geom} - E(S_1)^{S_1\,geom} \qquad (8)$$

1. M. J. Frisch, G. W. T., H. B. Schlegel, G. E. Scuseria, ; M. A. Robb, J. R. C., G. Scalmani, V. Barone, ; G. A. Petersson, H. N., X. Li, M. Caricato, A. V. Marenich, ; J. Bloino, B. G. J., R. Gomperts, B. Mennucci, H. P. Hratchian, ; J. V. Ortiz, A. F. I., J. L. Sonnenberg, D. Williams-Young, ; F. Ding, F. L., F. Egidi, J. Goings, B. Peng, A. Petrone, ; T. Henderson, D. R., V. G. Zakrzewski, J. Gao, N. Rega, ; G. Zheng, W. L., M. Hada, M. Ehara, K. Toyota, R. Fukuda, ; J. Hasegawa, M. I., T. Nakajima, Y. Honda, O. Kitao, H. Nakai, ; T. Vreven, K. T., J. A. Montgomery, Jr., J. E. Peralta, ; F. Ogliaro, M. J. B., J. J. Heyd, E. N. Brothers, K. N. Kudin, ; V. N. Staroverov, T. A. K., R. Kobayashi, J. Normand, ; K. Raghavachari, A. P. R., J. C. Burant, S. S. Iyengar, ; J. Tomasi, M. C., J. M. Millam, M. Klene, C. Adamo, R. Cammi, ; J. W. Ochterski, R. L. M., K. Morokuma, O. Farkas, ; J. B. Foresman, a. D. J. F. *Gaussian 16, Revision C.01,* , Wallingford CT,: Gaussian, Inc.,, 2019.
2. Becke, A. D., Density-functional exchange-energy approximation with correct asymptotic behavior. *Physical review A* **1988,** *38* (6), 3098.
3. Becke, A. D., Density-Functional Thermochemistry .III. The Role of Exact Exchange. *The Journal of Chemical Physics* **1993,** *98* (7), 5648−5652.
4. Becke, A. D., Density-functional thermochemistry. III. The role of exact exchange. *The Journal of chemical physics* **1993,** *98* (7), 5648-5652.
5. McLean, A.; Chandler, G., Contracted Gaussian basis sets for molecular calculations. I. Second row atoms, Z= 11–18. *The Journal of chemical physics* **1980,** *72* (10), 5639-5648.
6. Krishnan, R.; Binkley, J. S.; Seeger, R.; Pople, J. A., Self-consistent molecular orbital methods. XX. A basis set for correlated wave functions. *The Journal of chemical physics* **1980,** *72* (1), 650-654.
7. Jeffrey Hay, P.; Wadt, W., Ab initio effective core potentials for molecular calculations. Potentials for the transition metal atoms Sc to Hg. *J. Chem. Phys* **1985,** *82*, 270-283.
8. Chiodo, S.; Russo, N.; Sicilia, E., LANL2DZ basis sets recontracted in the framework of

density functional theory. *The Journal of chemical physics* **2006,** *125* (10), 104107.

9.      Adamo, C.; Barone, V., Toward reliable density functional methods without adjustable parameters: The PBE0 model. *The Journal of chemical physics* **1999,** *110* (13), 6158-6170.

10.     Ernzerhof, M.; Scuseria, G. E., Assessment of the Perdew–Burke–Ernzerhof exchange-correlation functional. *The Journal of chemical physics* **1999,** *110* (11), 5029-5036.

11.     Adamo, C.; Scuseria, G. E.; Barone, V., Accurate excitation energies from time-dependent density functional theory: Assessing the PBE0 model. *The Journal of chemical physics* **1999,** *111* (7), 2889-2899.

12.     Curtiss, L. A.; Raghavachari, K.; Redfern, P. C.; Pople, J. A., Investigation of the use of B3LYP zero-point energies and geometries in the calculation of enthalpies of formation. *Chemical physics letters* **1997,** *270* (5-6), 419-426.

13.     Barone, V.; Adamo, C., Proton transfer in the ground and lowest excited states of malonaldehyde: A comparative density functional and post-Hartree–Fock study. *The Journal of chemical physics* **1996,** *105* (24), 11007-11019.

14.     Ali, A.; Farid, T.; Rafiq, M. I.; Zhou, B.; Tang, W., Evaluating the impact of Hartree–Fock exact exchange on the performance of global hybrid functionals for the vertical excited-state energies of fused-ring electron acceptors using TD-DFT. *Physical Chemistry Chemical Physics* **2022,** *24* (35), 21270-21282.

15.     Ali, A.; Rafiq, M. I.; Zhou, B.; Tang, W., Evaluating the nature of the vertical excited states of fused-ring electron acceptors using TD-DFT and density-based charge transfer. *Physical Chemistry Chemical Physics* **2021,** *23* (28), 15282-15291.

16.     Hirata, S.; Head-Gordon, M., Time-dependent density functional theory within the Tamm–Dancoff approximation. *Chemical Physics Letters* **1999,** *314* (3-4), 291-299.

17.     Tomasi, J.; Mennucci, B.; Cammi, R., Quantum mechanical continuum solvation models. *Chemical reviews* **2005,** *105* (8), 2999-3094.

18.     Grimme, S.; Antony, J.; Ehrlich, S.; Krieg, H., A consistent and accurate ab initio parametrization of density functional dispersion correction (DFT-D) for the 94 elements H-Pu. *The Journal of chemical physics* **2010,** *132* (15), 154104.

19.     Wang, F.; Ziegler, T., A simplified relativistic time-dependent density-functional theory formalism for the calculations of excitation energies including spin-orbit coupling effect. *The Journal of chemical physics* **2005,** *123* (15), 154102.

20.     Te Velde, G. t.; Bickelhaupt, F. M.; Baerends, E. J.; Fonseca Guerra, C.; van Gisbergen, S. J.; Snijders, J. G.; Ziegler, T., Chemistry with ADF. *Journal of Computational Chemistry* **2001,** *22* (9), 931-967.

21.     Van Lenthe, E.; Ehlers, A.; Baerends, E.-J., Geometry optimizations in the zero order regular approximation for relativistic effects. *The Journal of chemical physics* **1999,** *110* (18), 8943-8953.

22.     Marcus, R. A., Electron transfer reactions in chemistry: theory and experiment (Nobel lecture). *Angewandte Chemie International Edition in English* **1993,** *32* (8), 1111-1121.

## 2. Single crystal X-ray analysis

**Table S1.** The crystallographic parameters and the structure refinement statistics for **1**, **2**, and **3**

| | 1 | 2 | 3 |
|---|---|---|---|
| Chemical formula | $C_{50}H_{41.5}ClCuN_{4.5}P_2$ | $C_{49.5}H_{40.75}BrCuN_{4.25}P_2$ | $C_{50}H_{41.5}CuIN_{4.5}P_2$ |
| Crystal system, space group | Triclinic, $P\bar{1}$ | | |
| Temperature (K) | 100 | 150 | 100 |
| $a$, (Å) | 10.4535(6), | 11.0522 (9), | 11.130 (3), |
| $b$, (Å) | 14.2480(7), | 13.1316 (9), | 13.148 (4), |
| $c$, (Å) | 16.8455(10) | 17.1379 (13) | 17.218 (7) |
| $\alpha$, (°) | 108.465(2), | 112.504 (2), | 67.595 (5), |
| $\beta$, (°) | 97.843(2), | 96.207 (3), | 73.923 (11), |
| $\gamma$, (°) | 111.0630(10) | 102.344 (3) | 77.448 (9) |
| $V$ (Å$^3$) | 2130.2(2) | 2194.5 (3) | 2220.4 (13) |
| $Z$ | 2 | 1 | 2 |
| Radiation type | Mo $K\alpha$ | | |
| $D_{calc}$ (g·cm$^{-3}$) | 1.351 | 1.363 | 1.433 |
| $m$ (mm$^{-1}$) | 0.69 | 1.52 | 1.30 |
| Crystal size (mm) | 0.35 × 0.34 × 0.3 | 0.18 × 0.1 × 0.1 | 0.15 × 0.12 × 0.1 |
| No. of measured, independent and observed [$I > 2s(I)$] reflections | 44030, 12437, 10343 | 27432, 13295, 7995 | 21978, 13299, 11004 |
| $R_{int}$ | 0.124 | 0.058 | 0.030 |
| $(\sin q/l)_{max}$ (Å$^{-1}$) | 0.759 | 0.714 | 0.617 |
| $R[F^2 > 2s(F^2)]$, $wR(F^2)$, $S$ | 0.050, 0.125, | 0.055, 0.128, | 0.038, 0.089, |

|  | 1.01 | 1.02 | 1.042 |
|---|---|---|---|
| No. of parameters | 538 | 541 | 541 |
| $\Delta\rho_{max}$, $\Delta\rho_{min}$ (e Å$^{-3}$) | 0.65, -0.88 | 0.69, -0.68 | 1.151, -1.796 |

**Table S2.** Selected geometric parameters for **1-3**

| Complex | | 1 | | 2 | | 3 |
|---|---|---|---|---|---|---|
| Bonds (Å) | Cu1-Cl1 | 2.4062(5) | Br1-Cu1 | 2.5173(5) | Cu1-I1 | 2.6602(7) |
| | Cu1-P1 | 2.2568(5) | Cu1-P1 | 2.2635(9) | Cu1-P1 | 2.2614(9) |
| | Cu1-P2 | 2.2642(6) | Cu1-P2 | 2.2536(9) | Cu1-P2 | 2.2586(9) |
| | Cu1-N1 | 2.1046(16) | Cu1-N1 | 2.091(3) | Cu1-N1 | 2.085(2) |
| Angles (º) | P1-Cu1-Cl1 | 104.320(19) | P1-Cu1-Br1 | 107.22(3) | P1-Cu1-I1 | 105.80(2) |
| | P1-Cu1-P2 | 124.51(2) | P2-Cu1-Br1 | 109.60(3) | P2-Cu1-I1 | 108.91(3) |
| | P2-Cu1-Cl1 | 106.012(19) | P2-Cu1-P1 | 124.66(3) | P2-Cu1-P1 | 125.76(2) |
| | N1-Cu1-Cl1 | 104.93(5) | N1-Cu1-Br1 | 104.97(7) | N1-Cu1-I1 | 106.62(6) |
| | N1-Cu1-P1 | 112.74(5) | N1-Cu1-P1 | 103.84(7) | N1-Cu1-P1 | 103.91(6) |
| | N1-Cu1-P2 | 102.73(5) | N1-Cu1-P2 | 104.78(7) | N1-Cu1-P2 | 104.43(6) |

**Table S3.** D-H…A interactions in crystals **1-3**.

| Interaction | D-H, Å | H…A, Å | D…A, Å | D-H-A, deg. |
|---|---|---|---|---|
| **1** | | | | |
| N4-H4...Cl1 (2-x, 1-y, 1-z) | 0.88 | 2.29 | 3.137(2) | 162 |
| C8-H8...Cl1 | 0.95 | 2.65 | 3.557(2) | 159 |
| **2** | | | | |
| N3-H3...Br1 (1-x, -y, 1-z) | 0.88 | 2.52 | 3.353(3) | 158 |

| 3 | | | | |
|---|---|---|---|---|
| N9-H9...I1 (1-*x*, -*y*, 1-*z*) | 0.98 | 2.56 | 3.522(4) | 166 |

**Table S4.** Selected parameters of π-π intermolecular interactions in **2** and **3** (the analysis was done using PLATON software [A.L.Spek, Acta Cryst. 2009, D65, 148-155]).

| Aromatic fragment I | Aromatic fragment J (symmetry index) | $C_g$-$C_g$, Å[a] | α, deg.[a] | $C_g$(I)_Perp, Å[a] | Slippage, Å[a] |
|---|---|---|---|---|---|
| **2** | | | | | |
| N2C42N4N3C43 (triazole) | C44->C49 (phenyl in L) (-*x*, -*y*, 1-*z*) | 3.694(2) | 1.23(18) | 3.5112(14) | 1.071 |
| C25->C30 (phenyl on PPh$_3$) | C25->C30 (phenyl in PPh$_3$) (2-*x*, 1-*y*, 1-*z*) | 3.492(2) | 0 | 3.2673(14) | 1.232 |
| **3** | | | | | |
| N8N9C10N11C7 (triazole) | C12->C17 (phenyl in L) (-*x*, -*y*, 1-*z*) | 3.654(2) | 2.26(13) | 3.4600(10) | 1.044 |
| C12->C17 (phenyl in PPh$_3$) | C12->C17 (phenyl in PPh$_3$) (2-*x*, -*y*, 1-*z*) | 3.534(2) | 0 | 3.3123(10) | 1.232 |

[a] $C_g$-$C_g$ = distance between ring centroids (Å); α = dihedral angle between planes I and J (deg.); $C_g$(I)_Perp = Perpendicular distance of Cg(I) on ring J (Å); Slippage = distance between Cg(I) and perpendicular projection of Cg(J) on ring I (Ang) (Å).
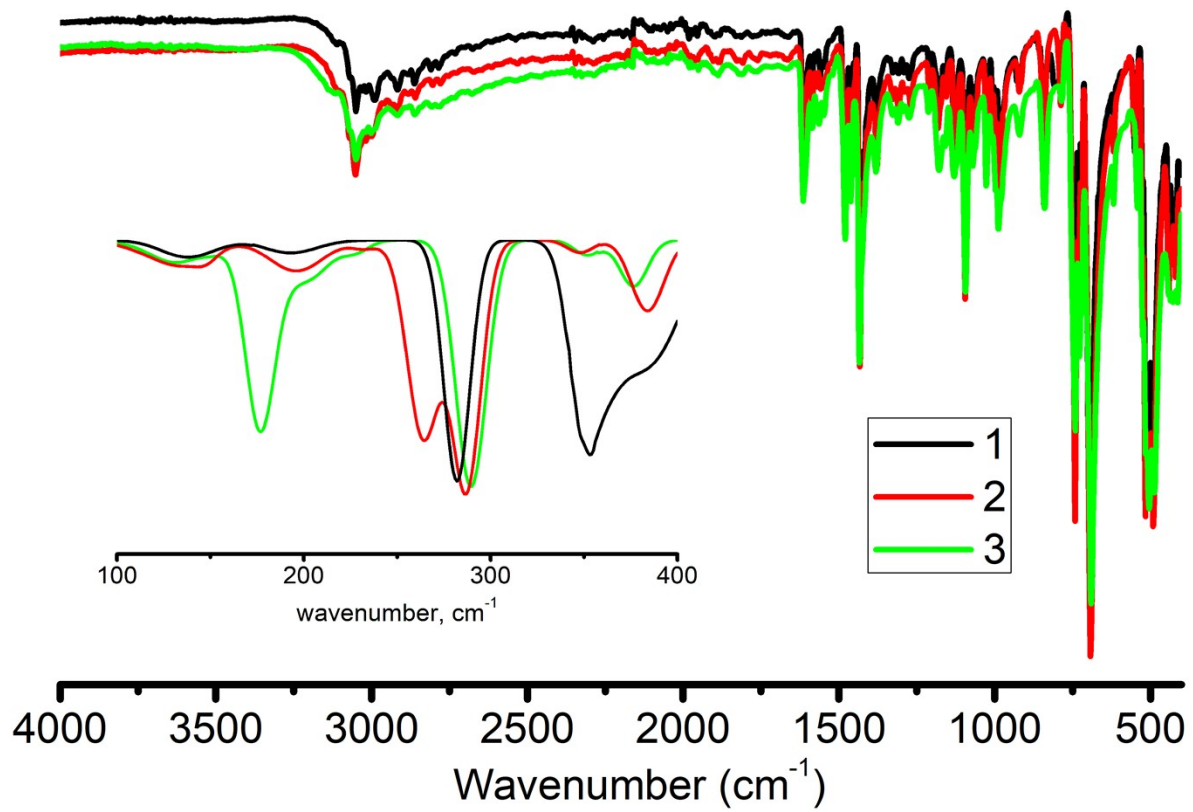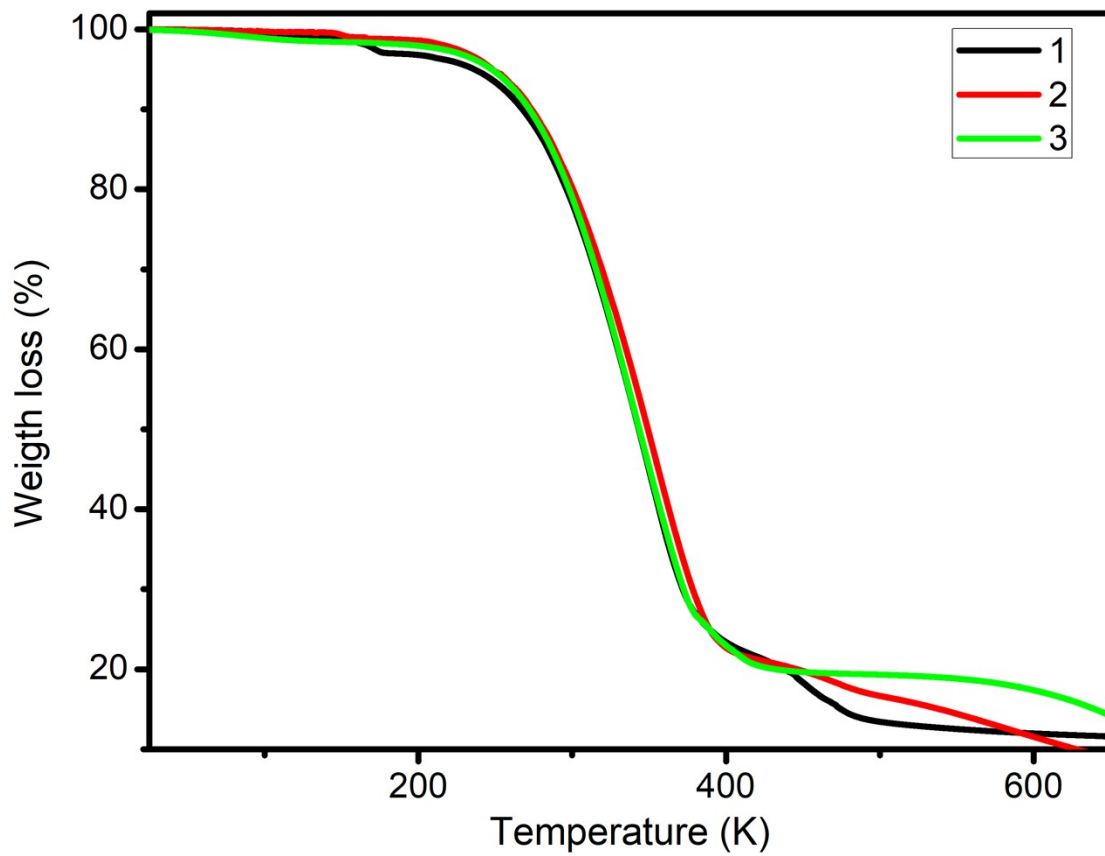
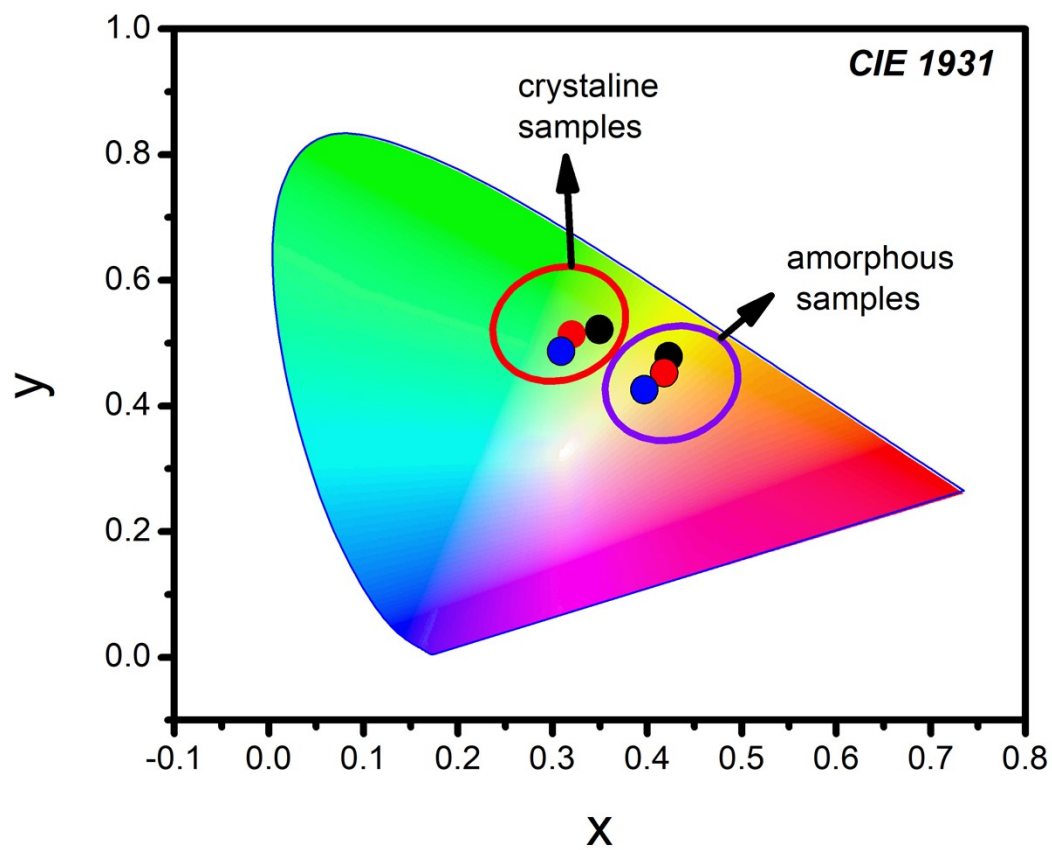Figure S1. IR-spectra of 1-3. Inset: Far-IR spectra

Figure S2. TGA curves of 1-3

Figure S3. CIE coordinates of crystalline and amorphous samples of 1 (black cycles), 2 (red cycles), 3 (blue cycles).

**Table S5.** Energies of frontier orbitals of 1-3 from electrochemical and optical data

| Device | LUMO (eV)[1] | HOMO (eV)[2] |
|---|---|---|
| Complex 1 | -2.28 | -5.30 |
| Complex 2 | -2.31 | -5.30 |
| Complex 3 | -2.34 | -5.32 |

1. Calculated from CV data by $E_{HOMO} = [(Eox-E1/2(ferrocene)+4.8]$
2. Calculated by $E_{LUMO} = E_{HOMO} + \Delta$. Where $\Delta$ – energy gap, obtained from spectral data

**OLED device fabrication**

Host injecting material poly(styrenesulfonate) (PEDOT:PSS, 1 : 6 dispersion in water, electronic grade AI4083), electron transport material of 1,3,5-tris[N-(phenyl)benzimidazole]benzene (TPBI) and the host material 2,6-bis(N-carbazolyl)pyridine (PYD-2Cz) were purchased from commercial sources and used without further purification.

The OLED devices were fabricated on glass substrates with 100 nm thickness ITO. A 40 nm thick PEDOT:PSS film was first spin-coated (at 5200 rpm) on a pre-cleaned ITO-glass substrate and then dried at 125 °C for 45 min. The emitting layer was then overlaid by spin coating (at 2500 rpm) a $CH_2Cl_2$ solution with the host and dopant (1 mg of complex 1, 2 or 3 and 9 mg of PYD2 in 10 mL of $CH_2Cl_2$). The obtained films were then dried under vacuum ($10^{-3}$ mbar) for 3 h at room temperature.

Layers of 3TPYMB (50 nm), LiF (1 nm), and 100 nm of Al were sequentially deposited at a rate in the range of 0.1-0.3 nm/s onto the substrates by high-vacuum ($10^{-5}$ mbar) thermal evaporation techniques. The shadow mask with 5 mm × 5 mm openings was used to define the cathodes. The evaporating speeds and thickness were monitored by quartz oscillators. The current density–luminance–voltage characteristics of the OLEDs were measured by Keithley source measurement unit with a calibrated silicon photodiode. Electroluminescence spectra were taken by a multichannel S2000 Ocean Optics spectrometer. All measurements were carried out in ambient atmosphere at room temperature.

.